Chemistry & Biology 13, 615–623, June 2006 DOI 10.1016/j.chembiol.2006.04.007

RNA-Selective, Live Cell Imaging Probes for Studying Nuclear Structure and Function

Qian Li,[1] Yunkyung Kim,[1] Joshua Namm,[1] Amita Kulkarni,[1] Gus R. Rosania,[2] Young-Hoon Ahn,[1] and Young-Tae Chang[1,*]
[1]Department of Chemistry
New York University
New York, New York 10003
[2]Department of Pharmaceutical Science
College of Pharmacy
University of Michigan
Ann Arbor, Michigan 48109

Summary

The higher-order structural organization of the cell nucleus reflects the underlying genome-wide transcriptional activity and macromolecular transport processes. To study the microscopic organization of RNA distribution within the nucleus, a combinatorial library of fluorescent styryl molecules was synthesized and screened for an in vitro RNA response and live cell nuclear imaging. Four different cell lines (HeLa, A549, 3T3, and 3T3-L1) were analyzed in terms of higher-order nuclear organization. We identified RNA-selective dyes with better imaging properties relative to commercially available SYTORNASelect dye; the selected dyes were also cell permeant, photostable, and well tolerated by the cells. Our dyes also had very good counterstain compatibility with Hoechst and DAPI, which could help to image the DNA distribution in relation to RNA distribution in live cells and therefore reveal different patterns of RNA-DNA colocalization.

Introduction

Live cell imaging with fluorescent microscopy technology has allowed for the investigation of the transcriptional dynamics of the cell nucleus [1, 2]. RNA molecules in living cells have been successfully visualized by using fluorescent-labeled RNA microinjection [3], fluorescence in situ hybridization (FISH) [4, 5], or the green fluorescence protein (GFP)- or its derivative (YFP)-tagged RNA binding proteins [6, 7]. However, the global dynamics of RNA distribution and transcriptional activity in the cell nucleus, in relation to the higher-order structural organization of the DNA, and the temporal and spatial processing and transportation of RNA molecules remains to be analyzed. To achieve this goal, a cell-permeant, RNA-selective fluorescent probe for staining live cells would be essential.

Small, cell-permeant, fluorescent organic molecules are widely used as probes to study living cells [8]. Although cell microinjection [3], GFP plasmid transfection [9], and other methods [10] used to introduce probes into the cells have their own advantages for specific study, small-molecule imaging probes are often the most practical tool for biological imaging research and medical diagnosis. Many fluorescent dyes are commercially available and stain a variety of living cell organelles such as the nucleus [11, 12], mitochondria [13], lysosomes [14], and endoplasmic reticulum [15]. In contrast, RNA-specific dyes for staining live cells are rarely available. SYTORNASelect [16] is the only commercially available dye for live cell RNA imaging, but its usefulness has not been proved widely. The molecular structure of SYTORNASelect dye has not been published yet either.

In the past, it has been shown that most of the RNA in the nucleus is localized to the nucleolus—a region of the nucleus that is clearly visible, by using phase contrast microscopy, as the densest, phase-dark region of the nucleus. The nucleolus is the key site in the nucleus that synthesizes and assembles the ribosomal RNAs (rRNA). Its functions are tightly related to cell growth and proliferation [17–19]. It is known that the nucleolar rRNA assembly takes place during late telophase and throughout interphase, and that the rRNAs dissemble when cells enter mitosis [20]. However, the details of nucleolar dynamic mechanisms of intracellular distribution, trafficking, and localization throughout a complete cell cycle are not known. Since it is difficult to study the nucleolar dynamics by using prefixed cells, a fluorescent, RNA-selective live cell imaging dye would be greatly advantageous in terms of allowing for the observation of changes in RNA content and distribution, in relation to the organization of DNA within the cell nucleus as revealed by known DNA-staining dyes.

Previously, we demonstrated that styryl dyes had good potential to become live cell fluorescence probes [21]. We have also found that some styryl dyes had good affinity for DNA [22]. However, finding RNA-selective dyes for live cell imaging is difficult, because small nucleic acid binding molecules generally have better affinity for double-stranded DNA than for single-stranded RNA. In addition, the living cell system is complicated by the fact that it is rich in proteins and membranes that may lead to nonspecific binding of hydrophobic imaging probes. Also, for imaging applications, the RNA binding dye needs to have high cell plasma and nuclear membrane permeability, needs to be well tolerated by living cells, and needs to be able to resist photobleaching. Surmounting these challenges, we report the successful identification of selective RNA binding fluorescent probes, by combining direct live cell screening with biochemical RNA fluorescence assays to screen newly synthesized, RNA-targeted styryl probes.

Results and Discussion

Synthesis and Characterization of the Styryl Dye Library

A new styryl dye library (1,336 members) was prepared for the current study. The synthesis followed the procedure we had developed previously, with slight modification [21] (Figure 1). Compared to the previous styryl dye library, we greatly expanded structural diversity by using more aldehydes as building block II (167 total, Figure S1, see the Supplemental Data available with

*Correspondence: yt.chang@nyu.edu

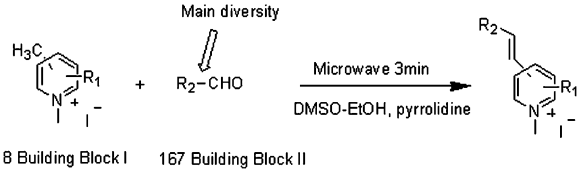

Figure 1. General Synthetic Scheme of Styryl Dyes

this article online; 41 aldehydes were used in the previous study), a decision guided by our previous experience with the development of specific DNA binding probes [22] from the starting library of nonspecific nuclear/nucleolar-staining [23] dyes. All of the aldehydes were commercially available. A huge variety of functional groups, such as higher conjugation groups, electron withdrawing and donating groups, acidic and basic groups, multiple functional groups, heterocyclic structure groups, and even polyaromatic structures, was included. The condensation reactions were accelerated by microwave irradiation for 3 min, which was catalyzed by pyrrolidine. The identity and purity of the products were characterized by LCMS (data not shown), and most reactions produced over 50% yields. More than 80% of the products showed a strong fluorescent property when tested in methanol, which allowed us to use this library in the primary screening without purification.

Primary and Secondary Screening

The screening strategy used in this study is shown in Figure 2. Both in vitro RNA assay and live cell imaging methods were utilized in the primary screening of the dye library. A good response of the dyes to RNA in solution was chosen as the primary criterion for selecting leads that may be most useful for bioimaging studies. Herein, the library dyes' fluorescent emission intensity fold change upon binding to RNA was measured in solution. Dyes showing five or more emission fold changes in the presence of RNA (Table S1) were selected (total of 42).

Meanwhile, the entire library was also screened directly by live cell imaging by using 3T3 fibroblast cells in a 50 μM concentration. A total of 46 dyes were identified based on selective localization of the fluorescent signal to cell nucleoli as well as on high signal intensity and low photobleaching (Table S2).

The selected compounds from both primary screens (total of 88) were resynthesized in large scale and purified. The compounds' live cell nuclear imaging properties were then tested by four cell lines, including two mouse cell lines—3T3 fibroblast cells and 3T3-L1 adipocyte cells—and two human cancer cell lines—HeLa cells and A549 human lung carcinoma cells. Herein, the final dye concentration in each test was decreased to 25 μM, and all of the experiments were repeated to establish reproducibility. From this secondary screening, the three best compounds (E36, E144, and F22) were finally selected based on their good nucleolar targeting, their high fluorescence intensity, low photobleaching, and the smallest effect on cell survival. We found that all three of the dyes contained at least one good nucleic acid affinity functional group [24–27] in building block II, such as a terminal secondary amine for F22, trimethoxy for E144, and indole for E36. Interestingly, they also compised a quinaldine or 6-methoxy quinaldine moiety; therefore, the quinaldine group may be important in live cell RNA structure targeting and cell permeability.

Characterization of the Three RNA-Selective Dyes

RNA Response in Solution

We have measured the detailed fluorescent properties of these three selected dyes: excitation/emission λ_{max}, the quantum yield, and the extinction coefficient of both the free dye solution and the dye-RNA solution (Table 1). All three dyes showed a significant quantum yield increase in RNA solution. Moreover, all of the dyes' excitation λ_{max}s showed a clear red shift (16 to 56 nm) in the

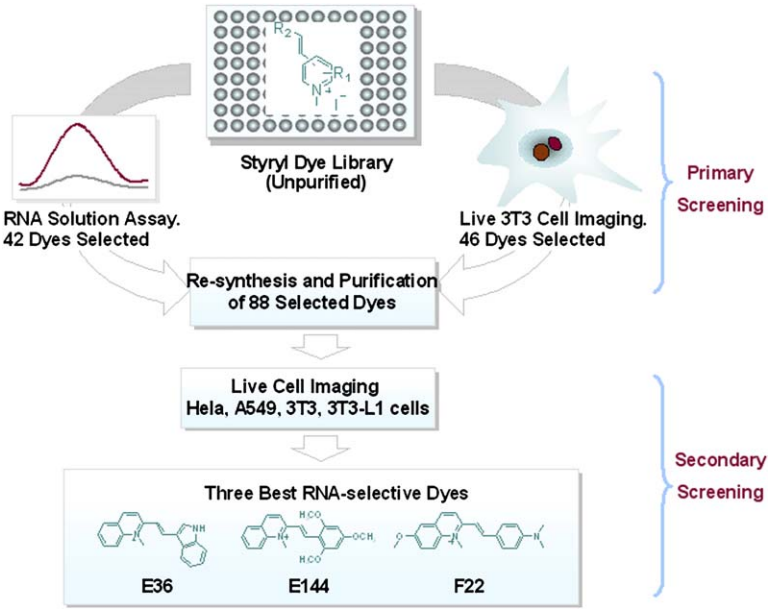

Figure 2. The Screening Strategy Used in This Study

Table 1. The Chemistry Structure of Three Selected Dyes, Their Solution Fluorescent Response to RNA, and the Optimum Concentration for Live Cell Imaging

Dye	Structure	EX/EM[a] (nm) Buffer	EX/EM[a] (nm) RNA	Φ_F^{free}[b]	Φ_F^{RNA}	$\Phi_F^{RNA}/\Phi_F^{free}$	ε^{free} ($M^{-1}cm^{-1}$)[c]	ε^{RNA} ($M^{-1}cm^{-1}$)	Optimum Concentration
E36	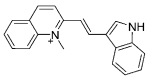	457/541	497/548	0.0019	0.1041	54.6	3.94×10^4	4.31×10^4	5 μM
E144	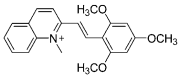	440/532	456/532	0.0056	0.0310	5.5	1.32×10^4	1.46×10^4	5 μM
F22	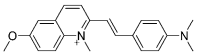	492/598	548/620	0.0007	0.0075	10.7	1.74×10^4	2.00×10^4	5 μM[d]

[a] Excitation and emission λ_{max} (nm) of three selected dyes were obtained by a Hitachi F-2500 FL fluorophotometer in TE buffer (pH 7.5). The final dye concentration was 5 μM, and the final RNA (16S- and 23S-ribosomal from *E. coli*) solution concentration was 200 μg/ml.
[b] Quantum yield was measured by a Gemini XS fluorescent plate reader in TE buffer (pH 7.5). Rhodamine 6G (5 μM) aqueous solution was used as a standard. The final dye concentration was 5 μM for E36 and 10 μM for E144 and F22. The final RNA solution concentration was 200 μg/ml.
[c] The extinction coefficient was measured by a SpectraMax Plus[384] absorbance plate reader. The solution condition was the same as that used for the quantum yield measurement.
[d] 3T3 cells could be imaged at 1 μM concentration.

presence of RNA, while the emission λ_{max}s remained similar.

In order to further study the RNA binding characteristics of these dyes, the dependence of fluorescent intensity based on the dye concentrations was then studied (Figure 3A). In the tested concentration range (0.15 μM to 10 μM for dye, 50 μg/ml for RNA), an obvious intensity increase was observed for all three dyes. An almost linear curve was obtained in the titration of E144, while E36 and F22 both showed evidence of saturation at high concentration. Moreover, a slight emission λ_{max} red shift was observed in E36 (total 8 nm) with an increasing concentration of dye. This may suggest a stacking binding mode of this dye to the RNA backbone [28]. Dyes E144

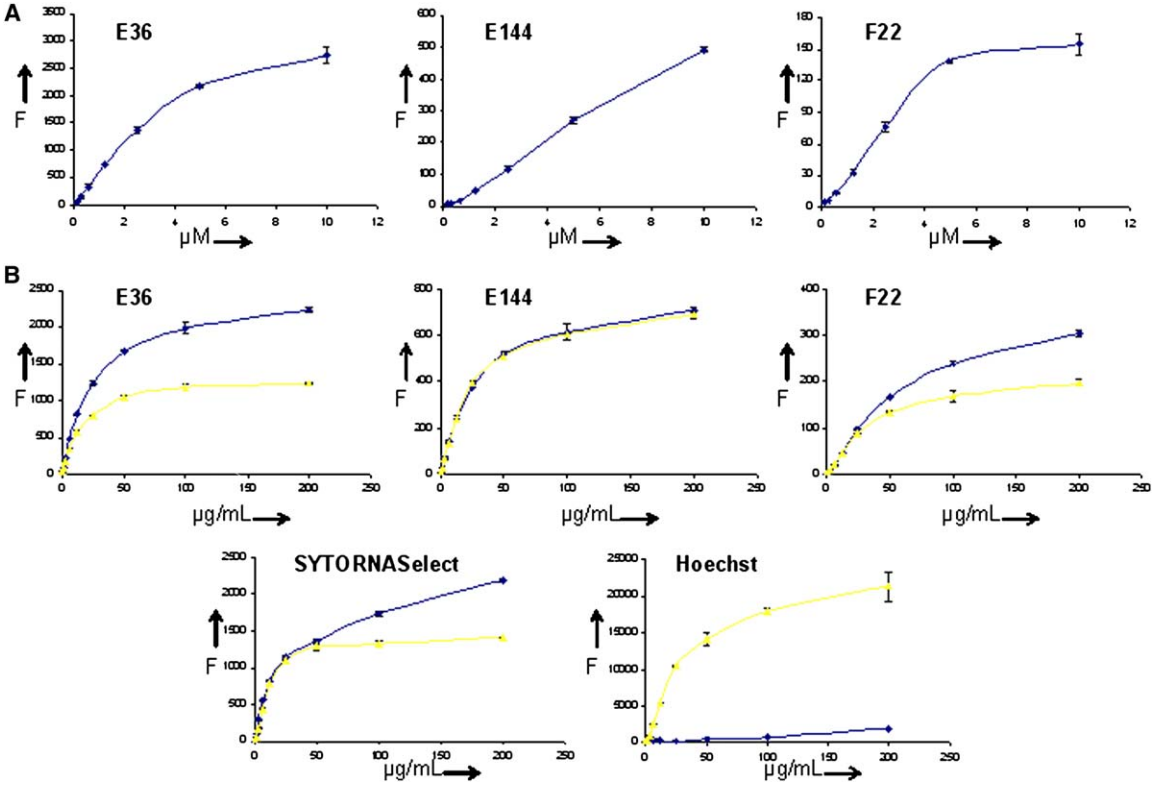

Figure 3. Selected Dyes' RNA and DNA Response in Solution

(A) Dye concentration dependency titration curve. Samples containing 50 μg/ml RNA in TE buffer with an increasing concentration of dye (from 0.15 μM to 10 μM). The intensity increase recorded at the emission λ_{max} wavelength of each dye is shown here.

(B) RNA (blue line) versus DNA (yellow line) selectivity titration curve. Samples containing a fixed concentration of dyes (E36, 5 μM; E144, 10 μM; F22, 10 μM) in TE buffer with an increasing concentration of RNA or DNA (from 0.19 μg/ml to 200 μg/ml). Data points were averaged from duplicate experiments, and error bars represent the standard deviation.

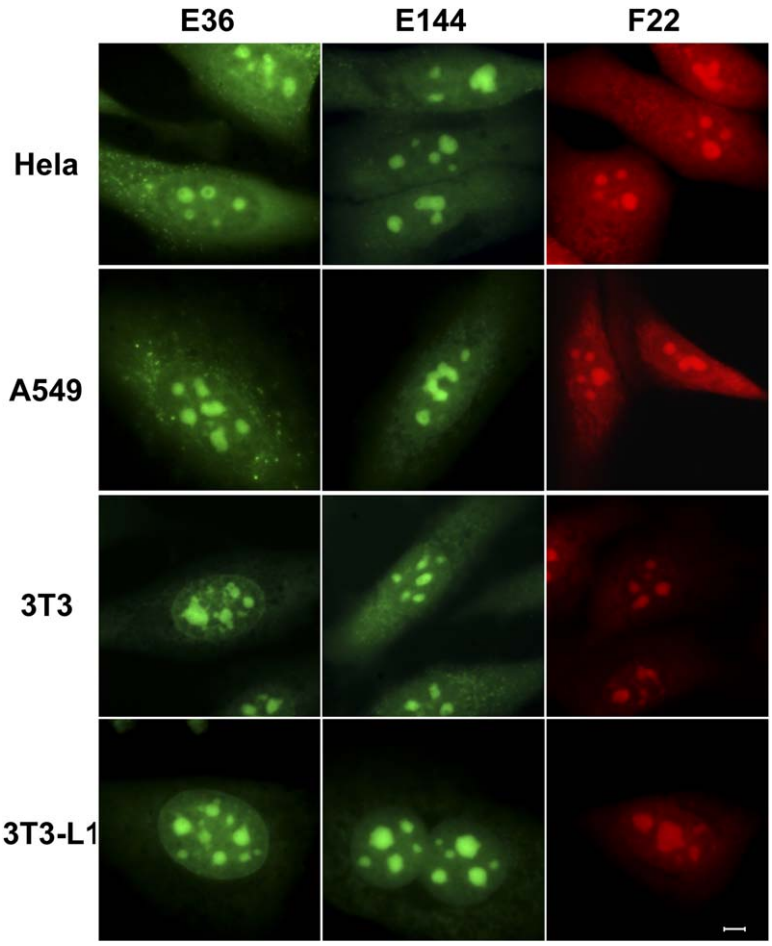

Figure 4. Live Cell RNA Staining with Selected Dyes

E36, E144, and F22 were tested at a 5 μM concentration. The picture of F22-stained 3T3 cells was obtained in a 1 μM dye concentration. 1000× magnification was utilized in the imaging. The scale bar represents 5 μm. Image brightness and contrast were slightly adjusted to improve picture quality. E36, E144 (green: FITC channel), and F22 (red: Cy3 channel) are shown.

and F22 did not show an obvious wavelength shift upon increasing dye concentrations.

Optimization of Dye Working Concentration and Imaging Properties

In fluorescence microscopic imaging studies, it is always desirable to use as little dye as possible to stain organelles, in consideration of specificity, dye toxicity, and interference with the cell viability. To determine the lowest working concentration of each dye, we tested these dyes in four different concentrations: 20 μM, 10 μM, 5 μM, and 1 μM for four cell lines (HeLa, A549, 3T3, and 3T3-L1). Dyes E36 and E144 were imaged by using the FITC channel, and F22 was imaged by using the Cy3 channel. Generally, we were able to get an efficient fluorescence signal of the stained cells at 5 μM for all three dyes (Table 1). It was interesting to observe that dye F22 was brighter in 3T3 cells, and that a 1 μM concentration was good enough for achieving a clear image (Figure 4). The dyes showed distinguishable clear nucleolar staining and faint nucleus and cytoplasm staining in all tested cell lines. Little photobleaching and no obvious cell morphology or viability change were found during the tests.

Live cell staining by SYTORNASelect had been reported recently [29]. Unfortunately, in this report, the staining of live cell RNA mainly stayed in the cytoplasm, and there was little staining in the nucleus. In our hands, a similar result was observed when using SYTORNASelect for the four cell lines and following the experimental protocol provided by the company (data not shown) (see http://probes.invitrogen.com for the staining protocol of SYTORNASelect). Therefore, although SYTORNASelect does stain fixed cell nucleoli [16, 30], it may not be good for live cell nucleolar RNA imaging applications. Clearly, the RNA-selective dyes reported in this study surpassed commercially available RNA probes in terms of their usefulness in live cell imaging experiments.

Dye Cell Tolerability

Low cytotoxicity is one of the most important criteria for live cell imaging probes. All three dyes were tested in four concentrations (20 μM, 13.5 μM, 10 μM, and 5 μM) in A549 cells and 3T3 cells, and the cytotoxicity was measured by using a standard MTS assay after 5, 15, or 24 hr of incubation (Figure S2A). Generally, after up to 24 hr of incubation, no toxicity (over 50% cell death) was found for all three dyes when their imaging working concentration (5 μM) was used. To the A549 cell, all three dyes remained nontoxic after 24 hr of incubation in all concentrations. To 3T3 cells, E144 had a similar nontoxic property, and toxicity was found with a high concentration (20 μM) of E36 and F22 after 24 hr and 15 hr of incubation, respectivley. Since RNA is the target of our dyes, it was not a surprise to see some signs of toxicity at higher concentrations, especially after one period of doubling time (~22 hr for A549 cells and 20–25 hr for 3T3 cells). Fortunately, the fact that toxicity is

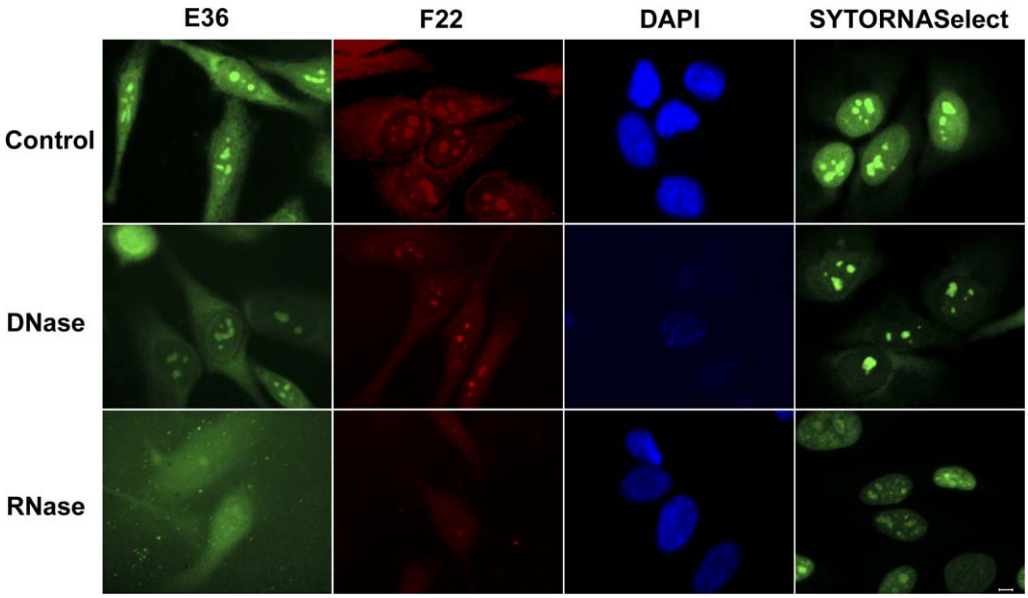

Figure 5. The DNase and RNase Digest Experiments

Images of E36, F22, as well as DAPI and SYTORNASelect are shown as comparison experiments; equal exposure was used for the same dye imaging. E36 and F22 were tested in a concentration of 50 μM. DAPI was tested in a concentration of 10 μM, and SYTORNASelect was tested in a concentration of 5 μM. 1000× magnification was utilized in the imaging. The scale bar represents 5 μm. The brightness and contrast of the control and DNase images of F22 were adjusted to improve picture quality. DAPI (blue: DAPI channel), E36 and SYTORNASelect (green: FITC channel), and F22 (red: Cy3 channel) are shown.

only apparent after very long incubation times at high dye concentration, and the fact that it is minimal at a lower, working concentration for all three dyes, ensures the applicability of these dyes as probes for imaging RNA distribution within cells. However, if the intention is to continuously visualize nucleolar dynamics throughout the cell cycle, then additional studies would be essential to establish that nucleolar dynamics are unperturbed.

Phototoxicity is also an important factor for evaluating the applicability of new fluorescent probes for live cell imaging. Phototoxicity is caused mainly by the direct absorption of high-energy UV light by the chromophores, or by the generation of a singlet oxygen due to the nonradiative energy transfer. Dyes that are excited by high-energy (violet-UV) wavelength light (such as Hoechst [31]) are most often prone to phototoxicity, although even longer wavelength dyes (such as FITC [32] and Rhodamine [33]) also exhibit light-induced toxicity if irradiated for prolonged periods of time. Nevertheless, it is desirable for the new imaging probes to be as little phototoxic as possible. To investigate our RNA-selective dyes, we tested the cell viability of irradiated cells by using the MTS assay. Cells were incubated with dyes in their working concentration (5 μM), and then irradiated with the appropriate filters by using the fluorescent microscope (FITC for E36 and E144; Cy3 for F22). While light exposures used for imaging experiments are generally a few seconds long at most, we irradiated the cells for 5 min to get a prolonged toxicity measurement. Irradiated cells were then incubated for 5 and 24 hr before being tested by the MTS assay. Both the cancer cell line (A549) and normal cell line (3T3) were tested in parallel (Figure S2B). In general, the toxicity was minimal. F22 showed photoxicity only to 3T3 cells (not to A549 cells) after 24 hr of incubation, but this effect was negligible at 5 hr of incubation. For comparison, we tested Hoechst 33258 (brief as Hoechst in the following) as a positive control, and we found that it was as toxic for 3T3 cells after up to 24 hr of incubation. Therefore, although it would be quite challenging to completely avoid phototoxicity, the phototoxicity of our styryl RNA probes is comparable and even lower than that of Hoechst, a broadly used, live cell imaging probe.

RNA versus DNA Specificity

A set of solution assay experiments were then carried out to investigate our dyes' selective response to RNA versus DNA in vitro. With a fixed concentration of dye (E36, 5 μM; E144, 10 μM; and F22, 10 μM), the fluorescent intensity in a range of different concentrations (0.195–200 μg/ml) of nucleic acids was obtained in their emission λ_{max} wavelength. SYTORNASelect (5 μM) and Hoechst (5 μM) dyes were measured as standards for RNA-selective and DNA-selective standard dyes as well (Figure 3B). When plotting the intensity changes with the increasing concentration of RNA or DNA, both E36 and F22 showed a higher response to RNA than to DNA, which corresponds to better nucleoli targeting in the live cell. Their RNA selectivity was comparable or higher than that of commercial SYTORNASelect. E144, however, showed almost the same binding affinity to both RNA and DNA.

To further confirm that our dyes selectively stain RNA in the cell, we performed a deoxyribonuclease (DNase) and ribonuclease (RNase) digest test. In the DNase digest, only the DNAs in the cell would be hydrolyzed. By contrast, in the RNase digest, only RNAs would be hydrolyzed. Fixed-permeabilized HeLa cells were used in this experiment, and DAPI and SYTORNASelect were also tested as controls (Figure 5). As expected,

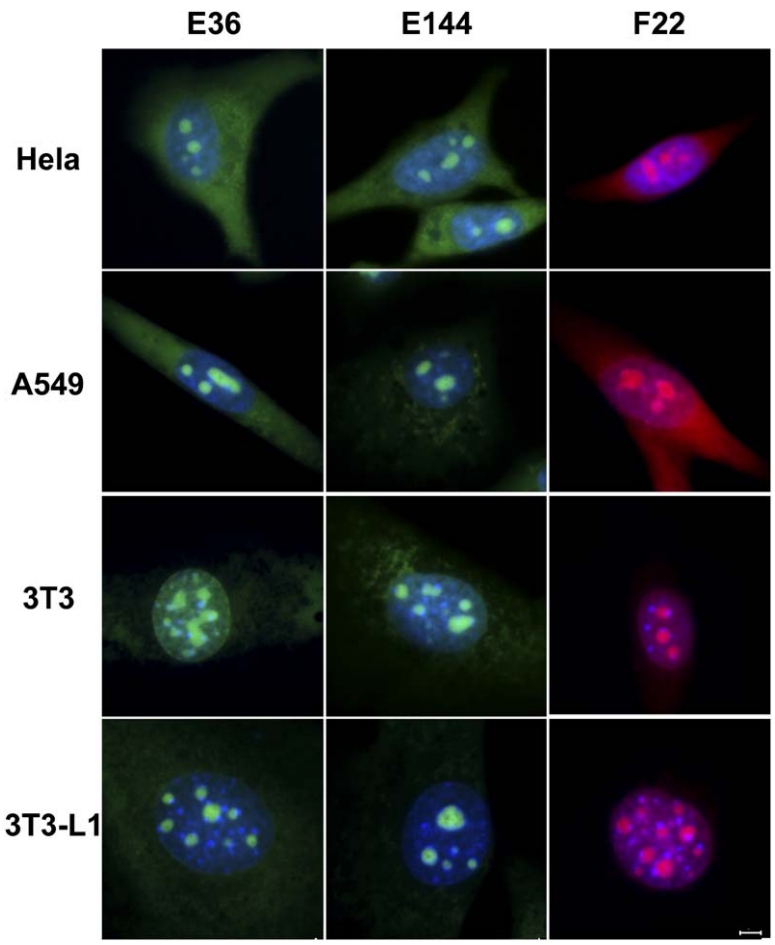

Figure 6. Live Cell Counterstain with Hoechst

E36, E144, and F22 were tested in a 5 μM concentration. The image of F22-stained 3T3 cells was obtained in a 1 μM dye concentration. A final concentration of 1 μM Hoechst was used for counterstain. 1000× magnification was utilized in the imaging. The scale bar represents 5 μm. Image brightness and contrast were adjusted to improve picture quality. E36, E144 (green: FITC channel), F22 (red: Cy3 channel), and Hoechst (blue: DAPI channel) are shown.

the fluorescence of dye E36 dramatically diminished in the RNase digest. However, with DNase, the nucleolar fluorescence intensity stayed almost the same as it was without treatment. Dye F22 showed obvious intensity diminishing in both DNase and RNase treatments; however, the nucleolar stain remained bright after the DNase treatment. The selective staining of dye E144 was not detectable after DNase and RNase experiments. It was observed that a dramatic decrease in fluorescence in E144 was also induced by the permeabilization process itself, which means that the detergent, Triton X-100, may interfere with the binding affinity between E144 and cell nucleic acids by removing the RNA-staining ability of this dye, or that it corresponded to its relatively low selectivity to RNA, previously shown in the solution test. Still, its higher RNA-selective binding in live cells might be due to the complicated in vivo live cell environment, which may preferably direct this dye to nucleoli. In short, although it is practically impossible to develop a 100% RNA-staining dye, the DNase and RNase experiments clearly demonstrated that the selectivity of these dyes is outstanding.

Counterstain Compatibility to Hoechst/DAPI and Determining Higher-Order Nuclear Organization

The classic live cell DNA-staining dyes Hoechst and DAPI have been widely used as DNA markers in the bioimaging field, and a good compatibility of our dyes with Hoechst and DAPI would be definitely helpful in the imaging of DNA and RNA distribution simultaneously. To study the higher-order nuclear organization of RNA molecules, cells stained with RNA-selective dyes need to be counterlabeled with a DNA-selective dye, such as Hoechst or DAPI. We established that all of our dyes were indeed orthogonal to Hoechst (Figure 6) and DAPI (Figure S3) when using DAPI-, FITC-, and Cy3-specific excitation/emission filter sets. We were able to clearly visualize the blue nucleus stain in the DAPI channel as well as our own dyes' nucleolar stain in either the FITC or Cy3 channel.

To address whether higher-order structural organization of the nucleus may be related to different patterns of transcriptional activity, we compared the distribution of DNA and RNA molecules in different cell lines. Remarkably, we found that the distribution of RNA-rich foci in relation to DNA-rich foci was largely cell type dependent. In 3T3-L1 cells, for example, DNA-rich foci were immediately juxtaposed to RNA-rich regions. In 3T3 cells, DNA-rich foci appeared to be randomly distributed with respect to RNA-rich regions. Lastly, in HeLa and A549 cells, DNA seemed to be distributed throughout the cell nucleus, whereas RNA foci still seemed to be as prominent and localized as they were in 3T3-L1 and 3T3 cells. This observation points to significant cell type-specific differences in RNA distribution, in relation to the condensation state of chromatin in different regions of the nucleus. Thus, there are significant

differences in higher-order organization that become immediately apparent upon microscopic observation of cells double-labeled with DNA and RNA-selective fluorescent probes.

Significance

We have discovered three fluorescent styryl dyes, E36, E144, and F22, that are highly specific, live cell RNA-staining molecules suitable for microscopic imaging and nuclear structural studies. These dyes have shown low cell cytotoxicity, low phototoxicity, and high photostability. Their fluorescence excitation/emission is orthogonal to commercially available DNA binding dyes, and they are found to be suitable for DNA-RNA colocalization experiments. Compared to SYTORNASelect, our dyes were more photostable and more selective, especially because of their clear ability to specifically stain RNA-rich foci within the live cell nucleus. In conclusion, these styryl dyes can open a new window into live cell microscopic imaging studies of nuclear structure and function.

Experimental Procedures

Materials and Instruments

Unless otherwise noted, chemical materials and solvents were purchased from commercial suppliers (Sigma-Aldrich and Acros) and were used without further purification. RNA (type VI from torula yeast, Sigma) was used for primary screening. RNA (16S- and 23S-ribosomal from *E. coli*, Roche) and DNA (from salmon testes, Sigma) were used in a solution response study for the best three selected dyes. TE buffer (Tris-EDTA sterile solution [pH 7.5], nuclease and protease-free 0.2 μm filtered solution, GE) was used in all solution experiments. A Gemini XS fluorescent plate reader was used in obtaining the excitation and emission spectra in the primary screening and selected dye titration assay studies. Greiner 96- or 384-well polypropylene black plates were used in the experiments. Full spectra data of the three selected dyes were obtained by a Hitachi F-2500 fluorophotometer. Absorbance spectra were measured with a SpectraMax Plus^{384} absorbance plate reader and Corning 384-well transparent plates. All dye compounds were identified by LC-MS (Agilent Technologies) by using a C18 column (4.6 × 150 mm) with a 4 min elution and a gradient of 5%–95% CH_3CN (containing 1% acetic acid)-H_2O (containing 1% acetic acid). The LC-MS contained a UV detector at λ = 250 nm, 350 nm, 430 nm, and 500 nm and an electrospray ionization source. Bruker Ultrashield 400 MHz NMR was used to obtain spectra of selected compounds. Human HeLa cells, A549 human lung carcinoma cells, mice 3T3-L1 cells, and 3T3 fibroblast cells were used in the cell staining study. A Leica confocal DMIRE2 fluorescent microscope was used in the imaging experiments. DAPI (ex 360/40, em 470/40, dichromatic filter 400), FITC (ex 480/40, em 527/30, dichromatic filter 505), and Cy3 (ex 545/30, em 610/75, dichromatic filter 565) band pass filter cubes (Chroma, www.chroma.com) were used for routine cell biological fluorescence imaging applications.

General Procedure for Synthesis of Building Block I

The pyridine derivative (2.04 mmol) and iodomethane (2.14 mmol) in ethyl acetate were refluxed overnight. After they were cooled to room temperature, the crystallized methylated products were filtered and washed with ethyl acetate three times and dried in a vacuum.

General Procedure for Synthesis of the Styryl Dye Library

Building blocks I and II were dissolved separately in absolute ethanol (100 mM) as stock solutions. In 96-well Gemini polypropylene microtiter plates, a 30 mM concentration of each reactant (30 μl DMSO and 0.1 μl pyrrolidine) was added with a multipipette. The condensation reaction was carried out in an 800 Watt microwave, and the reaction was carried out for 3 min for each plate. Product yield and purity were identified by LCMS.

General Procedure for Synthesis and Purification of 88 Selected Dye Compounds

In a 20 ml vial, building blocks I (0.1 mmol) and II (0.3–0.5 mmol) was dissolved together in 10 ml absolute ethanol. A total of 3 μl pyrrolidine was added to the solution. The condensation reaction was carried out by using a heating block at 80ºC for 3–6 hr. After the reaction was completed, the mixture stood at room temperature overnight. Purification was carried out by two different methods depending on the compounds. For the crystallized compounds, the crystal was filtered and recrystallized in ethanol and dried in a vacuum. Non-crystallized compounds were purified by silica preparative TLC or column chromatography with a ratio of methanol:methylene chloride of 1:10. (Solvent gradient polarity might be different depending on the compounds). All purified compounds were identified by LCMS, and an average of 95% purity was determined at the 250 nm absorption wavelength. Note that compound E36 was the deacylated indole product. The structure and purity of the selected final three compounds were confirmed by ^{1}H NMR (400 MHz, Methyl-d3, alcohol-d, and Chloroform-d) before the detailed cell staining study was performed (Supplemental Data).

For collaborative research purposes, the dye materials are available upon request.

General Fluorescence and Absorbance Spectra Measurement

The fluorescence spectra data in the primary screening and selected dye titration assay study were obtained with a Gemini XS plate reader. The RNA solution was prepared right before the assay experiments were performed to avoid possible degradation and contamination. In the primary screening, 1 mg/ml RNA (type VI from torula yeast) buffer solution was used. Point scans were carried out first by using five Ex/Em point sets (350/450, 400/500, 450/550, 500/600, 550/650 nm). Spectra scans were then carried out for the selected dyes. Excitation wavelengths were set at 350 nm, 400 nm, 450 nm, 500 nm, and 550 nm and the emission wavelengths were scanned. The three best selected dyes' RNA (16S- and 23S-ribosomal from *E. coli*, Roche) and DNA (from salmon testes, Sigma) titration experiments and quantum yield/extinction coefficient determination were carried out by the plate reader as well. The excitation λ_{max} obtained from a F-2500 Hitachi Fluorophotometer was used. The absorbance wavelength was determined by using a SpectraMax Plus^{384} absorbance plate reader. Rhodamine 6G was chosen as standard, and 480 nm was used as the excitation wavelength in the scanning for quantum yield determination.

General Fluorescence Spectra Measurement with an F-2500 Hitachi Fluorophotometer

Final concentrations of 5 μM of the selected dye and 200 μg/ml of RNA in TE buffer were used in the experiments. Generally, the λ_{max} (nm) of emission was determined by scanning a fixed excitation first, and the λ_{max} (nm) of excitation was determined by scanning emission spectrum with a fixed λ_{em} (nm).

Cell Culture Condition

HeLa, 3T3 fibroblast, and 3T3-L1 cells were grown on cell culture Petri dishes in Dulbecco's modified Eagle's medium (Sigma) with 10% newborn calf serum plus 5 mM L-glutamine and 5 μg/ml gentamicin. A549 cells were grown in Ham's F12 medium with 10% newborn calf serum plus 5 mM L-glutamine and 5 μg/ml gentamicin. Cell cultures were maintained in an incubator at 37ºC with 5% CO_2. Cells were cultured in glass bottom, 96-well black plates for imaging 12–24 hr prior to conduction of experiments.

Live Cell Staining

All cell staining imaging followed the same procedure. Generally, dyes in the dry state were first dissolved in DMSO to obtain the stock solution. The stock solutions were then added directly to the cell culture wells to reach the desired concentration. Total DMSO was lower than 0.1%. After adding dyes, cells were incubated at 37ºC in 5% CO_2 for 25 min. The medium was then removed, and cells were rinsed with fresh medium twice. The cells were then imaged at

ambient temperature in the medium. Exposure time was kept at less than 5 s and were adjusted for each dye.

Cytotoxicity Test

Dye DMSO stock solutions were diluted by fresh medium into four desired concentrations (20, 13.5, 10, and 5 μM). Cells were cultured in a 96-well plate for 12 hr before the conduction of the experiments. The cell medium was then exchanged by different concentrations of dye medium solutions. They were then incubated at 37ºC in 5% CO_2 for 5, 15, or 24 hr before cell viability was measured by the MTS assay. As for the MTS assay, briefly, 3-(4,5-dimethylthiazol-2-yl)-5-(3-carboxymethoxyphenyl)-2-(4-sulfophenyl)-2*H*-tetrazolium (MTS) and phenazine methosulfate (PMS) were mixed at a ratio of 20:1 right before the experiments were conducted. The cell dye medium solution was exchanged by 80 μl of fresh medium, followed by the addition of 20 μl MTS/PMS solution to each well. A total of 100 μM hydrogen peroxide was used as a positive control. The cell plates were then incubated at 37ºC in 5% CO_2 for 2 hr. Absorbance was measured at 490 nm. The absorbance measured for an untreated cell population under the same experimental conditions was used as the reference point to establish 100% cell viability. Duplicated experiments have been tested.

Phototoxicity Test

Dye DMSO stock solutions were diluted by fresh medium into a working concentration (5 μM). Cells were cultured in a 96-well plate for 12 hr before experiments were conducted. The cell medium was then exchanged by dye medium solutions. They were then incubated at 37ºC in 5% CO_2 for 25 min before being irradiated by fluorescent light by using a proper working filter (FITC for E36 and E144; Cy3 for F22) for 5 min. The plates were then incubated at 37ºC in 5% CO_2. The cell viability was measured by the MTS assay after 5 and 24 hr by following the cytotoxicity measurement procedure. Duplicated experiments have been tested.

DNase and RNase Digest Test

Cells were first fixed by −4ºC pure methanol for 1 min at ambient temperature. The cell membrane was then permeabilized by immersing the cell in 1% Triton X-100 for 2 min. After rinsing with PBS twice, 100 μl 50 μM dye PBS solution was added into three adjacent wells. Cells were then incubated in this dye PBS solution for 15 min in ambient temperature before being rinsed by clean PBS twice. A total of 100 μl clean PBS (as control experiment), 30 μg/ml DNase (Sigma), or 25 μg/ml DNase-Free RNase (GE) was added into the three adjacent wells and incubated at 37ºC in 5% CO_2 for 2 hr. Cells were rinsed by clean PBS twice more before imaging. For each dye test, the fluorescent imaging pictures were obtained by using an equal exposure time for control, Dnase, and RNase experiments. DAPI was made in 10 μM PBS solution for the test. SYTORNASelect was made in 5 μM PBS solution for the test. Duplicate experiments have been tested.

Live Cell Counterstain with Hoechst/DAPI

Cells were first stained in the desired concentration by following the previous staining procedure. After rinsing with fresh, prewarmed medium, Hoechst stock solution was added to the medium to obtain a 1 μM final concentration. Cells were then incubated at 37ºC in 5% CO_2 for 10 min and imaged at ambient temperature in the medium. The imaging of DAPI counterstain followed the similar procedure. The final concentration of DAPI was 5 μM. Prior to imaging, the cells were rinsed by fresh medium twice after 20 min of incubation with DAPI.

Supplemental Data

Supplemental Data including dye compound characterization, library building blocks, an MTS assay, DAPI cell counterstaining images, and solution library primary screening data are available at http://www.chembiol.com/cgi/content/full/13/6/615/DC1/.

Acknowledgments

We gratefully acknowledge the support of the National Science Foundation (CHE-0449139) and the National Institutes of Health (NIH) (RO1-GM078200). We also acknowledge equipment grants for the NMR (MRI-0116222) and the Capillary LC-Ion Trap Mass spectrometer (CHE-0234863). Components of this work were conducted in a Shared Instrumentation Facility constructed with support from Research Facilities Improvement Grant C06 RR-16572 from the National Center for Research Resources/NIH.

Received: January 20, 2006
Revised: March 24, 2006
Accepted: April 17, 2006
Published: June 23, 2006

References

1. Tsien, R.Y., and Miyawak, A. (1998). Seeing the machinery of live cells. Science *280*, 1954–1955.
2. Stephens, D., and Allan, V.J. (2003). Light microscopy techniques for live cell imaging. Science *300*, 82–86.
3. Mhlanga, M.M., Vargas, D.Y., Fung, C.W., Kramer, F.R., and Tyagi, S. (2005). tRNA-linked molecular beacons for imaging mRNAs in the cytoplasm of living cells. Nucleic Acids Res. *33*, 1902–1912.
4. Femino, A.M., Fay, F.S., Fogarty, K., and Singer, R.H. (1998). Visualization of single RNA transcripts in situ. Science *280*, 585–590.
5. Dirks, R.W., Molenaar, C., and Tanke, H.J. (2003). Visualizing RNA molecules inside the nucleus of living cells. Methods *29*, 51–57.
6. Andersen, J.S., Lam, Y.W., Leung, A.K.L., Ong, S.-E., Lyon, C.E., Lamond, A.I., and Mann, M. (2005). Nucleolar proteome dynamics. Nature *433*, 77–83.
7. Bertrand, E., Chartrand, P., Schaefer, M., Shenoy, S.M., Singer, R.H., and Long, R.M. (1998). Localization of ASH1 mRNA particles in living yeast. Mol. Cell *2*, 437–445.
8. Johnson, I. (1998). Fluorescent probes for living cells. Histochem. J. *30*, 123–140.
9. Zhang, J., Campbell, R.E., Ting, A.Y., and Tsien, R.Y. (2002). Creating new fluorescent probes for cell biology. Nat. Rev. Mol. Cell Biol. *3*, 906–918.
10. McNeil, P.L., and Warder, E. (1987). Glass beads load macromolecules into living cells. J. Cell Sci. *88*, 669–678.
11. Martin, R.M., Leonhardt, H., and Cardoso, M.C. (2005). DNA labeling in living cells. Cytometry A *67*, 45–52.
12. Krishan, A., and Dandekar, P.D. (2005). DAPI fluorescence in nuclei isolated from tumors. J. Histochem. Cytochem. *53*, 1033–1036.
13. Pendergrass, W., Wolf, N., and Poot, M. (2004). Efficacy of MitoTracker Green and CMXrosamine to measure changes in mitochondrial membrane potentials in living cells and tissues. Cytometry A *61*, 162–169.
14. Rustom, A., Saffrich, R., Markovic, I., Walther, P., and Gerdes, H.H. (2004). Nanotubular highways for intercellular organelle transport. Science *303*, 1007–1010.
15. Mironov, S.L., Ivannikov, M.V., and Johansson, M. (2005). $[Ca^{2+}]i$ signaling between mitochondria and endoplasmic reticulum in neurons is regulated by microtubules. From mitochondrial permeability transition pore to Ca^{2+}-induced Ca^{2+} release. J. Biol. Chem. *280*, 715–721.
16. Haulgland, R.P. (2005). Assays for cell viability, proliferation and function. In The Handbook, A Guide to Fluorescent Probes and Labeling Technologies Tenth Edition, M.T.Z. Spence, ed. (Eugene, Oregon: Invitrogen, Molecular Probes), pp. 710–711.
17. Lam, Y.W., Trinkle-Mulcahy, L., and Lamond, A.I. (2005). The nucleolus. J. Cell Sci. *118*, 1335–1337.
18. Olson, M.O., Hingorani, K., and Szebeni, A. (2002). Conventional and non-conventional roles of the nucleolus. Int. Rev. Cytol. *219*, 199–266.
19. Carmo-Fonseca, M., Mendes-Soares, L., and Campos, I. (2000). To be or not to be in the nucleolus. Nat. Cell Biol. *2*, E107–E112.
20. Hernandez-Verdun, D., Roussel, P., and Gebrane-Younes, J. (2002). Emerging concepts of nucleolar assembly. J. Cell Sci. *115*, 2265–2270.
21. Rosania, G.R., Lee, J.W., Ding, L., Yoon, H.S., and Chang, Y.T. (2003). Combinatorial approach to organelle-targeted

fluorescent library based on the styryl scaffold. J. Am. Chem. Soc. *125*, 1130–1131.
22. Lee, J.W., Jung, M., Rosania, G.R., and Chang, Y.T. (2003). Development of novel cell-permeable DNA sensitive dyes using combinatorial synthesis and cell based screening. Chem. Commun. *15*, 1852–1853.
23. Shedden, K., Brumer, J., Chang, Y.T., and Rosania, G.R. (2003). Chemoinformatic analysis of a supertargeted combinatorial library of styryl molecules. J. Chem. Inf. Comput. Sci. *43*, 2068–2080.
24. Trotta, E., and Paci, M. (1998). Solution structure of DAPI selectively bound in the minor groove of a DNA T·T mismatch-containing site: NMR and molecular dynamics studies. Nucleic Acids Res. *26*, 4706–4713.
25. Loontiens, F.G., Regenfuss, P., Zechel, A., Dumortier, L., and Clegg, R.M. (1990). Binding characteristics of Hoechst 33258 with Calf Thymus DNA, Poly[d(A-T)], and d(CCGGAATTCCGG): multiple stoichiometries and determination of tight binding with a wide spectrum of site affinities. Biochemistry *29*, 9029–9039.
26. Zipper, H., Brunner, H., Bernhagen, J., and Vitzthum, F. (2004). Investigations on DNA intercalation and surface binding by SYBR Green I, its structure determination and methodological implications. Nucleic Acids Res. *32*, E103.
27. Glazer, A.N., and Rye, H.S. (1992). Stable dye-DNA intercalation complexes as reagents for high-sensitivity fluorescence detection. Nature *359*, 859–861.
28. Sovenyhazy, K.M., Bordelon, J.A., and Petty, J.T. (2003). Spectroscopic studies of the multiple binding modes of a trimethine-bridged cyanine dye with DNA. Nucleic Acids Res. *31*, 2561–2569.
29. Santangelo, P., Nitin, N., LaConte, L., Woolums, A., and Bao, G. (2006). Live-cell characterization and analysis of a clinical isolate of bovine respiratory syncytial virus, using molecular beacons. J. Virol. *80*, 682–688.
30. Voss, M.R., Gupta, S., Stice, J.P., Baumgarten, G., Lu, L., Tristan, J.M., and Knowlton, A.A. (2005). Effect of mutation of amino acids 246–251 (KRKHKK) in HSP72 on protein synthesis and recovery from hypoxic injury. Am. J. Physiol. Heart Circ. Physiol. *289*, H2519–H2525.
31. Libbus, B.L., Perreault, S.D., Johnson, L.A., and Pinkel, D. (1987). Incidence of chromosome aberrations in mammalian sperm stained with Hoechst 33342 and UV-laser irradiated during flow sorting. Mutat. Res. *182*, 265–270.
32. Rumbaut, R.E., and Sial, A.J. (1999). Differential phototoxicity of fluorescent dye-labeled albumin conjugates. Microcirculation *6*, 205–213.
33. Shea, C.R., Sherwood, M.E., Flotte, T.J., Chen, N., Scholz, M., and Hasan, T. (1990). Rhodamine 123 phototoxicity in laser-irradiated MGH-U1 human carcinoma cells studied in vitro by electron microscopy and confocal laser scanning microscopy. Cancer Res. *50*, 4167–4172.